Efficient quantum dynamics simulations of complex molecular systems: A unified treatment of dynamic and static disorder

Efficient Quantum Dynamics Simulations of Complex Molecular Systems: a Unified Treatment of Dynamic and Static Disorder

Maxim F. Gelin,[1, a)] Amalia Velardo,[2] and Raffaele Borrelli[2, b)]

[1)] *School of Sciences, Hangzhou Dianzi University, Hangzhou 310018, China*

[2)] *DISAFA, University of Torino, Grugliasco I-10095, Italy*

(Dated: 15 February 2023)

We present a unified and highly numerically efficient formalism for the simulation of quantum dynamics of complex molecular systems which takes into account both temperature effects and static disorder. The methodology is based on the Thermo-Field Dynamics formalism and Gaussian static disorder is included into simulations via auxiliary bosonic operators. This approach, combined with the Tensor-Train/Matrix-Product States representation of the thermalized stochastic wave function, is applied to study the effect of dynamic and static disorder in charge-transfer processes in model organic semiconductor chains employing the Su-Schrieffer-Heeger (Holstein-Peierls) model Hamiltonian.

Keywords: Thermo-Field Dynamics, Dynamic Disorder, Static Disorder, Tensor-Trains, Matrix-Product-States, Charge-Transfer

[a)]Electronic mail: maxim@hdu.edu.cn

[b)]Electronic mail: raffaele.borrelli@unito.it

I. INTRODUCTION

The measurement of chemico-physical properties of real molecular systems is always affected by thermal motion and inherent static disorder of the microscopic degrees of freedom (DoFs) of matter.[1] Thermal motion having a characteristic timescale comparable to that of the observable under examination generates dynamic disorder, while static disorder originates from the presence of uncorrelated fluctuations of microscopic structural parameters whose values have a significant dispersion but do not change substantially during the observation time. Recent research has clearly demonstrated that understanding the way in which dynamic and static disorder affect molecular properties is of utmost importance for the design and development of new materials for organic photovoltaics in particular and for energy transport and transduction in general.[2]

A common approach to include static disorder effects in the evaluation of the desired property is to average the result of a quantum dynamical simulation over a large number of realizations of the microscopic system.[3,4] Similarly, thermal motion, *i.e.* dynamic disorder, is often treated either within the reduced density matrix framework,[5,6] or with an explicit full quantum treatment of thermalized DoFs of interest,[7] that again requires a sampling of the initial thermal distribution of the system. In both cases, when the sampling space becomes very large, these approaches might become cumbersome and inefficient. The existing analytical methods of performing static disorder averaging can be applied in certain limiting cases only (see Ref.[8] and references therein). It is therefore instrumental to develop computationally efficient and numerically accurate approaches to simulate quantum dynamics of realistic systems that can take into account both thermal motion and static disorder effects. Recently, we have proposed an alternative approach to describing quantum dynamics of complex molecular systems in a thermal environment which is based on the so-called Thermo-Field Dynamics (TFD) theory,[9–14] combined with a very efficient Tensor-Train (TT) representation of the thermal wave function[15] (see also Ref.[16] for a recent review). The main advantage of the this TFD-TT methodology is that it provides a thermally averaged property with a single propagation of an extended wave function,[9,17] and its effectiveness in studying fundamental chemico-physical processes and in simulating non-linear spectroscopic signals has been clearly demonstrated.[10,11,18,19]

Here we extend the TFD-TT theoretical framework to treat both thermal and static dis-

order on equal footing, in order to accurately evaluate the expectation value of any dynamic variable averaged over static disorder with a single time-dependent simulation of an extended thermal Schrödinger-like equation. More specifically, we present an efficient theoretical and computational method for the simulation of time-dependent properties of quantum electron-vibrational systems with many DoFs that can take into account both thermal motion of low frequency vibrations, and static disorder of the electronic DoFs. Thermal motion is described using a temperature dependent formulation of the Schrödinger equation which has been recently developed by Borrelli and Gelin,[9] and static disorder is accurately treated via the stochastic Liouville equation.[6,20] Within this formalism a generalized wave function is used to compute, with just a single time propagation, thermal and static disorder averaged properties of observables. We further show how to take advantage of recently developed techniques based on Tensor Networks to solve the resulting dynamical problem.[21] In particular we demonstrate that the TT decomposition[21–24], also known as Matrix Product State (MPS) representation, can provide a robust and efficient numerical tool for the solution of the TFD Schrödinger equation, and enables the treatment of static disorder with a minimal computational extra cost. Applications of the new computational framework are presented and discussed in section IV.

II. STOCHASTIC EFFECTS IN FINITE-TEMPERATURE SCHRÖDINGER EQUATION

The aim of this section is to derive a new Schrödinger-like equation that describes the evolution of a collection of quantum systems at finite temperature, whose characteristic parameters show a certain degree of disorder. More specifically we assume that the system dynamics can be described by a vibronic coupling (VC) model. These models, in which diabatic potential energy surfaces are represented by polynomials of nuclear coordinates, are commonly used for the construction of *ab initio*-based Hamiltonians of polyatomic chromophores[25,26], molecular aggregates[27–31] and molecular materials[32,33]. The VC models can also be efficiently interfaced with classical trajectory simulations[34]. Usually, diagonal terms in the diabatic potential energy surfaces of VC Hamiltonians are retained up to the second order in nuclear coordinates (harmonic approximation), while off-diagonal inter-state couplings are assumed to be either coordinate independent (constant VC (CVC) models de-

scribing avoided crossings between diabatic electronic states) or linear in nuclear coordinates (linear VC (LVC) models describing conical intersections between diabatic electronic states). VC Hamiltonians usually contain high-frequency Franck-Condon-active vibrational modes (which are strongly coupled to electronic states) as well as relevant low-frequency vibrational modes responsible for thermal effects. For definiteness, here we consider a generic CVC model Hamiltonian in which electronic energies and couplings have a certain degree of disorder. LVC and other higher-order polynomial VC Hamiltonians can be treated in the same manner.

The generalized CVC Hamiltonian can be written as follows:

$$H_\Omega = \sum_{n,m} \left(\varepsilon_{nm} + \sum_j V^j_{nm} \sigma_j \Omega_j + \sum_k \frac{g_{knm}}{\sqrt{2}} (a^\dagger_k + a_k) \right) |n\rangle\langle m| + \sum_k \omega_k a^\dagger_k a_k. \tag{1}$$

Here $|n\rangle$ are the electronic states, ε_{nm} are the electronic energies ($n = m$) and couplings ($n \neq m$), $a^\dagger_k$ (a_k) are the creation (annihilation) operators of the kth harmonic mode with frequency ω_k, g_{nmk} are the electron-vibrational coupling parameters, Ω_j are dimensionless random variables, σ_j are the dispersion parameters quantifying static disorder (precise meaning of σ_j is clarified below), and V^j_{nm} specify coupling of Ω_j to the electronic subsystem. For a given quantum observable A we wish to evaluate its expectation value

$$\mathcal{A}(t) = \int d\Omega \langle A_\Omega(t) \rangle \tag{2}$$

where $\langle A_\Omega(t) \rangle$ represents the expectation value for a single realization of Ω,

$$\langle A_\Omega(t) \rangle = \mathrm{Tr}(\rho_\Omega(t) A),$$

and the density matrix $\rho_\Omega(t)$ satisfies the Liouville – von Neumann equation ($\hbar = 1$)

$$\partial_t \rho_\Omega(t) = -i[H_\Omega, \rho_\Omega(t)] \tag{3}$$

with the initial condition

$$\rho_\Omega(0) = |e\rangle\langle e| \rho_v P_\Omega. \tag{4}$$

Here $|e\rangle$ is a certain initial excited electronic state,

$$\rho_v = Z_v^{-1} \exp\{-\beta \sum_k \omega_k a^\dagger_k a_k\}, \tag{5}$$

is the equilibrium Boltzmann vibrational distribution (Z_v is the partition function, $\beta = (k_B T)^{-1}$, k_B is the Boltzmann constant, and T is the temperature), and P_Ω is the probability

density of static disorder variables Ω_j. We assume that P_Ω is described by a Gaussian distribution with unit dispersion,

$$P_\Omega = \prod_j \frac{1}{\sqrt{2\pi}} e^{-\Omega_j^2/2}. \tag{6}$$

With this definition, the variables $\sigma_j \Omega_j$ possess a Gaussian distribution with dispersion σ_j. Hence the term $V_{nm}^j \sigma_j \Omega_j$ in the Hamiltonian of Eq. (1).

Following a common approach originally formulated within the stochastic Liouville equation formalism (see, e.g., Ref.[6]) we treat stochastic disorder variables as harmonic oscillator coordinates and write

$$\Omega_j = (z_j^\dagger + z_j)/\sqrt{2}$$

where $z_j^\dagger$ (z_j) are the creation and annihilation operators of the jth disorder parameter. Then the Hamiltonian of Eq. (1) assumes the form

$$H_\Omega = \sum_{n,m} \left(\varepsilon_{nm} + \sum_j V_{nm}^j \frac{\sigma_j}{\sqrt{2}} (z_j^\dagger + z_j) + \sum_k \frac{g_{knm}}{\sqrt{2}} (a_k^\dagger + a_k) \right) |n\rangle\langle m| + \sum_k \omega_k a_k^\dagger a_k \tag{7}$$

and Eq. (2) can be rewritten as

$$\mathcal{A}(t) = \langle 0_\Omega | \langle A_\Omega(t) \rangle | 0_\Omega \rangle \tag{8}$$

where $|0_\Omega\rangle$ is the ground state wave function of the multi-dimensional harmonic oscillator

$$|0_\Omega\rangle = \prod_j \frac{1}{\sqrt[4]{2\pi}} e^{-\Omega_j^2/4} \tag{9}$$

so that

$$P_\Omega = |0_\Omega\rangle\langle 0_\Omega|. \tag{10}$$

We have thus reformulated, in absolutely equivalent manner, the original problem by employing the second quantization representation for disorder variables Ω_j.

At this point, the general TFD scheme developed in Refs.[9,10,17] can be readily applied to the Liouville – von Neumann equation (3) driven by the Hamiltonian of Eq. (7). The details of the derivation can be found in the Appendix and the final is given below. The disorder averaged expectation value can be expressed as

$$\mathcal{A}(t) = \langle 0_\Omega | \langle \mathbf{0}_v \tilde{\mathbf{0}}_v | \langle e | e^{iH_\theta t} A_\theta e^{-iH_\theta t} | e \rangle | \mathbf{0}_v \tilde{\mathbf{0}}_v \rangle | 0_\Omega \rangle \tag{11}$$

where H_θ is the Hamiltonian H_Ω of Eq. (7) after the thermal Bogoliubov transformation[10],

$$H_\theta = \sum_k \frac{\omega_k}{2}\left(a_k^\dagger a_k - \tilde{a}_k^\dagger \tilde{a}_k\right) + \tag{12}$$

$$\sum_{n,m}\left(\varepsilon_{nm} + \sum_j V_{nm}^j \frac{\sigma_j}{\sqrt{2}}(z_j^\dagger + z_j) - \sum_k \frac{g_{knm}}{\sqrt{2}}\left\{\left(a_k + a_k^\dagger\right)\cosh(\theta_k) + \left(\tilde{a}_k + \tilde{a}_k^\dagger\right)\sinh(\theta_k)\right\}\right)|n\rangle\langle m|,$$

and

$$\theta_k = \operatorname{arctanh}(e^{-\beta\omega_k/2}). \tag{13}$$

Here were have introduced the creation (annihilation) operators $\tilde{a}_k^\dagger$ ($\tilde{a}_k$) of the auxiliary (so-called tilde) vibrational modes which, according to the TFD formalism, take care of temperature effects and $|\mathbf{0}_v\tilde{\mathbf{0}}_v\rangle$ is the collective ground (vacuum) state for both physical (a_k, $a_k^\dagger$) and tilde ($\tilde{a}_k$, $\tilde{a}_k^\dagger$) vibrational DoFs. The Bogoliubov-transformed operator A_θ is defined by Eq. (A16). If the original operator A depends on electronic DoFs only (this is the case for the system studied below) then $A_\theta = A$.

Equivalently, Eq. (11) can be rewritten as

$$\mathcal{A}(t) = \big\langle\psi_\theta(t)\big|A_\theta\big|\psi_\theta(t)\big\rangle \tag{14}$$

where the wave function $\big|\psi_\theta(t)\big\rangle$ satisfies the TFD Schrödinger equation

$$i\partial_t\big|\psi_\theta(t)\big\rangle = H_\theta\big|\psi_\theta(t)\big\rangle \tag{15}$$

with the initial condition

$$\big|\psi_\theta(0)\big\rangle = |e\rangle|\mathbf{0}_v\tilde{\mathbf{0}}_v\rangle\big|0_\Omega\big\rangle. \tag{16}$$

The TFD Schrödinger equation (15) is fully equivalent to the original Liouville – von Neumann equation (3). The number of vibrational modes in H_θ is double of that in the original Hamiltonian H_Ω of Eq. (1), and electron-vibrational couplings in H_θ are renormalized by temperature-dependent factors: $\cosh(\theta_k)$ for physical vibrational modes and $\sinh(\theta_k)$ for tilde vibrational modes. If $T \to 0$ then $\theta_j \to 0$, the coupling to the tilde space disappears, and the standard Schrödinger equation is recovered as expected. Nonzero temperature causes dynamical mixing of physical (a_k, $a_k^\dagger$) and tilde ($\tilde{a}_k$, $\tilde{a}_k^\dagger$) variables. It is essential that the disorder modes (z_k, $z_k^\dagger$) are not doubled, because averaging over variables Ω_j with the Gaussian distribution of Eq. (6) is fully equivalent to the vacuum averaging of the disorder oscillators according to Eq. (10). Notice also that kinetic terms corresponding to disorder

modes are missing in H_Ω and H_θ. This literally reflects static nature of the disorder modes which can be interpreted as intra- or inter-molecular nuclear modes whose frequencies tend to zero. This observation demonstrates logical consistency of the combined treatment of static and dynamic disorder. Summarizing, only vibrational DoFs are doubled in the TFD Schrödinger equation (15), while the number of the electronic DoFs and the number of disorder oscillators remains unchanged.

Let N_{el}, N_v, and N_Ω be the number of the electronic, vibrational, and static disorder DoFs in the original Hamiltonian of Eq. (1). Then traditional evaluation of $\mathcal{A}(t)$ via the Liouville – von Neumann equation (3) requires M_Ω propagations of the density matrix $\rho_\Omega(t)$ for the system with N_{el} electronic and N_v vibrational DoFs, where $M_\Omega \gg N_\Omega$ is the number of Monte Carlo samplings necessary for the calculation of the N_Ω-dimensional integral (2) over the static disorder variables Ω_j. Evaluation of $\mathcal{A}(t)$ via the TFD Schrödinger equation (15) requires just a single propagation of the wave function $\left|\psi_\theta(t)\right\rangle$ for the system with N_{el} electronic and $2N_v + N_\Omega$ vibrational DoFs. As we will show in the next section the time propagation can be performed using extremely efficient methods based on the TT/MPS formalism leading to enormous computational savings in the calculation of expectation values of operators averaged over static disorder.

III. TENSOR TRAINS/ MATRIX PRODUCT STATES

The solution of the TFD Schrödinger equation (15) with the Hamiltonian of Eq. (12) requires efficient numerical methods, suitable to accurately treat a large number of dynamical variables. Several techniques have been developed which can, at least in principle, overcome what has been termed the *curse of dimensionality*.[15,35] In our approach the Tensor-Train (TT) decomposition, the simplest form of Tensor Network, has been adopted. Below we sketch the basic principles of the TT decomposition, and show how it can be applied to solve the thermal Schrödinger equation in twin-formulation. The reader is referred to the original papers[15,22,36] for a detailed analysis of the TT theory.

Let us consider a generic state $|\psi\rangle$ of a N dimensional quantum system having the form

$$|\psi\rangle = \sum_{i_1,i_2,...,i_N} C(i_1,...,i_N)\,|i_1\rangle\,|i_2\rangle\cdots|i_N\rangle\,. \tag{17}$$

where $|i_k\rangle$ labels the basis states of the kth dynamical variable, and the elements $C(i_1,...,i_N)$

are complex numbers labeled by N indices. If we truncate the summation of each index i_k the elements $C(i_1, ..., i_N)$ represent a tensor of order N. The evaluation of the summation in Eq. (17) requires the computation (and storage) of p^N terms, where p is the average size of the one-dimensional basis set that is usually much larger than 2. This becomes prohibitive for large N. Using the TT format, each element $C(i_1, ..., i_N)$ of the tensor C is approximated as

$$C(i_1, ..., i_N) \approx C_1(i_1)C_2(i_2)\cdots C_N(i_N) \tag{18}$$

where each $C_k(i_k)$ is a $r_{k-1} \times r_k$ complex matrix. In the explicit index notation

$$C(i_1, ..., i_N) \approx$$

$$\sum_{\alpha_0\alpha_1\cdots\alpha_N} C_1(\alpha_0, i_1, \alpha_1)C_2(\alpha_1, i_2, \alpha_2)\cdots C_N(\alpha_{N-1}, i_N, \alpha_N) = \sum_{\{\alpha_k\}}\prod_{k=1}^{N} C_k(\alpha_{k-1}, i_k, \alpha_k) \tag{19}$$

The matrices C_k are three dimensional arrays, called *cores* of the TT decomposition. The dimensions r_k are called compression ranks, that in the MPS language are referred to as *bond dimensions*. Since the product of Eq. (18) must be a scalar, the constraint $\alpha_0 = \alpha_N = 1$ must be imposed. Using the TT decomposition of Eq. (18) it is possible, at least in principle, to overcome most of the difficulties caused by the dimensionality problem. Indeed, the wave function is entirely defined by N arrays of dimensions $r_{k-1} \times n_k \times r_k$ thus requiring a storage dimension of the order Npr^2.

The TT approximation is effective only if the ranks r_k of the cores are small. The structure of the train, that is the order of the indices of the tensor, can have a deep impact on the growth of the entanglement. A key aspect is that if two DoFs are highly entangled their indices should be as close as possible in the sequence that defines the TT representation of the wave function. The most desirable situation would correspond to a systems showing only nearest neighbor interactions and a structure of the tensor train that reflects the natural form of the Hamiltonian operator.

Several techniques exist to map the Hamiltonian of Eq. (12) to chain-like models, thus easing the application of the TT format.[37–39] It has been recently demonstrated, however, that this mapping might not be necessary at all, and sometimes can even be counterproductive.[40] In all the applications of the present work we have found that ordering of the electronic and vibrational DoFs of the Hamiltonian in Eq. (A14) with increasing values of their frequency ω_i provides very good convergence properties of the TT representation,

and the mapping to a chain form is not required.

The TT cores of a time-dependent wave function are time dependent complex-valued matrices which must be determined from the numerical solution of the equations of motion of the system.[23,24,41] The simplest possible approach to tackle this problem is to use standard integrators of systems of ordinary differential equations combined with the TT algebra.[24] Fast Fourier Transform techniques have also been successfully exploited.[42] An alternative method is based on the application of the Dirac-Frenkel time-dependent variational principle (TDVP) to the parametrised form of the state given by Eq. (18).[43] Since TTs of fixed rank form a closed manifold $\mathcal{M}_{TT}$ the resulting equations of motion can be written in the form

$$\frac{d}{dt}\big|\psi(C(t))\big\rangle = -i\hat{P}_{\mathcal{T}(\psi(C(t)))}H\big|\psi(C(t))\big\rangle, \tag{20}$$

where C labels all the cores of the TT representation (18), and $\hat{P}_{\mathcal{T}(\psi(C(t)))}$ is the orthogonal projection into the tangent space of $\mathcal{M}_{TT}$ at $\big|\psi(C(t))\big\rangle$. Eq. (20) provides an approximate solution of the original equation on the manifold of TTs of fixed rank, $\mathcal{M}_{TT}$.[36] This means that the projected evolution gives the best solution with a prescribed upper bound for the ranks of the cores. This strategy is extremely appealing because it avoids, by construction, the growth of the ranks of the TT solution. The drawback of the methodology is that the accuracy of the solution must be verified *a posteriori*: Several calculations with increasing values of the TT ranks r_k should be performed until a global convergence on a desired observable is reached.

We refer the reader to Refs.[23,44,45] for a discussion of time-dependent TT/MPS approximations. The results presented in section IV have been obtained with an in-home code developed using the TDVP algorithm.

IV. APPLICATION TO CHARGE-TRANSFER IN ORGANIC SEMICONDUCTORS

The theoretical framework developed in the preceding section has a wide range of applications and, as already pointed out, it is not limited to CVC/LVC models but can be applied to a much wider class of Hamiltonian operators. It is of particular interest to show how it can be exploited to study the interplay between static and dynamics disorder effects in model organic semiconductor systems. More specifically we consider a molecular chain

comprised of identical sites with nearest-neighbour couplings in which the inter-site couplings are modulated by the low frequency modes of the sites, and the site energies have a certain degree of static disorder. This situation, that is widespread in a variety of molecular aggregates,[46,47] can be formalized employing the so-called Su-Schrieffer-Heeger (SSH) VC Hamiltonian,[48]

$$H_\Omega = \sum_{n=1}^{N_{el}} (\omega_{x_n} a_{x_n}^\dagger a_{x_n} + \omega_{y_n} a_{y_n}^\dagger a_{y_n}) + \tag{21}$$

$$\sum_{n=1}^{N_{el}} \left(\varepsilon + \sigma_n \Omega_n + g x_n\right) |n\rangle\langle n| + \sum_{n=1}^{N_{el}-1} \left(J + \alpha(y_n - y_{n+1})\right) \left(|n\rangle\langle n+1| + |n+1\rangle\langle n|\right).$$

Here $x_n = (a_{x_n} + a_{x_n}^\dagger)/\sqrt{2}$ denotes the vibrational coordinate with frequency ω_{x_n} localized on site n and $y_n = (a_{y_n} + a_{y_n}^\dagger)/\sqrt{2}$ is the transversal coordinate with frequency ω_{y_n}. We assume that the SSH chain is comprised of identical sites and the state energy ε, electron-vibrational intra-state coupling g, electronic inter-state coupling J and vibronic inter-state coupling α are n-independent. We further assume that static disorder affects only site energies and the variances are independent of n, $\sigma_n = \sigma$. The values of the system parameters adopted in the simulations are given in Table I. These values are representative for a wide class of oligoacene derivatives exhibiting the common vynil stretch around 1300 cm^{-1} with a reorganization energy of about 557 cm^{-1} which falls within the range usually associated to organic semiconductors.[49] This model has been widely employed in the literature to describe charge-transport phenomena in oligoacene systems.[50,51] Effects of static disorder on the site energies, that from a physical point of view can be caused by solid state imperfections, are often neglected in the study of the mechanistic aspects of the charge-transfer (CT) processes in molecular crystals.[52] Here we study the behaviour of the charge delocalization dynamics as a function of the degree of static disorder σ and of the temperature for a $N_{el} = 10$ site SSH model system.

The TT-TDVP calculations were performed for several values of the bond dimension until convergence of the desired populations was reached. More specifically, we consider the calculation fully converged if the time averaged relative error of a given property, *i.e.* the site populations, falls below a given threshold, which in the present case is set to 0.01. Our calculations show that an average value of the bond dimension close to 120 guarantees the required convergence on the specified time interval.

We assume that the population at $t = 0$ is localized in site 1 ($p_1(0) = 1$, $p_k(0) = 0$ for

TABLE I. Numerical values (in cm^{-1}) of the parameters of the SSH Hamiltonian used in the simulations of the present work.

ω_x	ω_y	g	J	α	σ
1300	50	1200	300	100, 300	0, 100, 300

$k \neq 1$). In order to provide a concise and clear analysis of the CT mechanism we report the behavior of three quantities: electronic populations $p_k(t)$, the inverse participation ratio (IPR)[10,53–56]

$$\Pi(t) = \left[\sum_{k=1}^{N_{el}} p_k(t)^2\right]^{-1} \tag{22}$$

and the second moment

$$m_2(t) = \frac{1}{N_{el}} \sum_{k=1}^{N_{el}} k^2 \langle p_k \rangle . \tag{23}$$

$p_k(t)$ gives a direct view of the CT process. $\Pi(t)$ provides a simple visualization of the charge delocalization, being 1 for a completely localized state and N_{el} for a charge delocalized over N_{el} sites. $m_2(t)$ is used to classify different CT regimes. Indeed, the square root of this quantity frequently follows a power law of the type $\sqrt{m_2(t)} \propto t^\nu$ where $\nu = 0$ corresponds to complete localization, $\nu = 1/2$ corresponds to a classical small-step diffusion, $\nu = 1$ corresponds to ballistic motion, $\nu \in (0, 1)$ corresponds to anomalous diffusion, and $\nu > 1$ corresponds to superballistic motion. In complex dynamical processes, the parameter ν is not constant, and the type of dynamics can be described as piecewise ballistic or diffusive according to the approximate value of ν in a specific time interval.

It is convenient to characterize the initial decay of the expectation values of quantum observables by so-called Zeno time τ_Z which is defined through the formula[57]

$$\mathcal{A}(t) = \exp\{-(t/\tau_Z)^2\} + O(t^3).$$

As shown in Refs.[19,58], Zeno rate $\nu_Z \equiv \tau_Z^{-1}$ can be calculated analytically for VC Hamiltonians. Applying this analysis to $p_1(t)$, one obtains:

$$\nu_Z^2 = J^2 + \alpha^2 \left(\langle y_1^2 \rangle + \langle y_2^2 \rangle\right) = J^2 + \alpha^2 \left(1 + \frac{2}{\exp\{\beta\omega_y\} - 1}\right). \tag{24}$$

Zeno rate ν_Z increases with temperature: it is minimal at $T = 0$ ($\nu_Z = \sqrt{J^2 + \alpha^2}$) , reaches the value $\nu_Z = \sqrt{J^2 + \alpha^2 2k_B T/\omega_y}$ in the classical limit $k_B T \gg \omega_y$ and becomes $\sim \sqrt{T}$ for

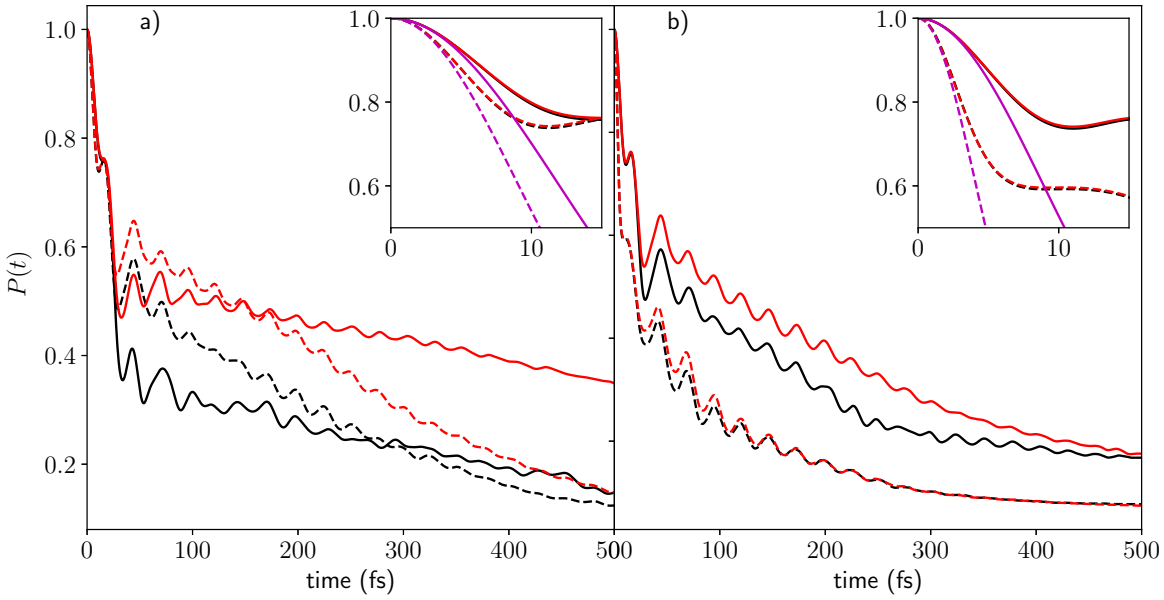

FIG. 1. Population of site 1, $p_1(t)$ for $\alpha = 100$ cm^{-1} (a) and $\alpha = 300$ cm^{-1} (b). $\sigma = 0$, $T = 0$ (continuous black line), $\sigma = 300$ cm^{-1}, $T = 0$ (continuous red line), $\sigma = 0$, $T = 300$ K (dashed black line), $\sigma = 300$ cm^{-1}, $T = 300$ K (dashed red line). Insets show the initial dynamics on an enlarged scale and the Zeno-time evolutions (pink lines).

$\alpha^2 2k_BT/\omega_y \gg J^2$, yielding $\nu_Z = \alpha\sqrt{2k_BT/\omega_y}$. The initial decay of $p_1(t)$ is thus independent of static disorder and high-frequency modes. It is specified by the interstate coupling constants J and α as well as by the low-frequency mode ω_y which is responsible for the temperature dependence of ν_Z.

We begin with the analysis of site populations. Fig. 1 shows evolution of the initially populated site, $p_1(t)$, for weak ($\alpha = 100$ cm^{-1}, a)) and relatively strong ($\alpha = 300$ cm^{-1}, b)) modulation of the interstate vibronic coupling by the low-frequency mode ω_y. Each panel displays $p_1(t)$ without static disorder ($\sigma = 0$, black lines) and with relatively strong static disorder ($\sigma = 300$ cm^{-1}, red lines) at $T = 0$ K (continuous lines) and 300 K (dashed lines).

Let us first consider panel a) which corresponds to $\alpha = 100$ cm^{-1}. The $p_1(t)$ curves reveals two global characteristic times: Zeno time τ_Z of the order of ten femtoseconds and a σ-dependent changeover time τ_{ch} of the order of several hundreds of femtoseconds at which the dashed and the continuous curves intersect (*see infra*). The short-time ($t < \tau_Z$) dynamics of $p_1(t)$ is shown in the inset of Fig. 1. It is consistent with the predictions of

Eq. (24): black lines (no static disorder) and red lines (strong static disorder) coincide for the same temperature, while continuous lines corresponding to $\tau_Z = 16.8$ fs at $T = 0$ K are above dashed lines corresponding to $\tau_Z = 12.7$ fs at $T = 300$ K. Notice also that the Zeno curves calculated via Eq. (24) reproduce $p_1(t)$ on the timescale of a few femtoseconds, due to the substantially non-Gaussian evolution of $p_1(t)$ at longer times. For $t > \tau_Z$, depopulation of $p_1(t)$ decreases with static disorder (continuous/dashed red lines go above the corresponding black lines), which is a manifestation of the disorder-induced localization. As for the temperature, the behavior is richer. For $\tau_{ch} > t > \tau_Z$ ($\tau_{ch} \approx 150$ fs for red curves and $\tau_{ch} \approx 270$ fs for black curves) depopulation of $p_1(t)$ decreases with temperature (continuous lines are below the dashed lines of the same color) while for $t > \tau_{ch}$ this tendency is inverted. This reveals two major effects due to the increase of temperature. On the one hand, it makes the system more classical, increases irreversibly, and opens more channels for the energy transfer. This facilitates the onset of irreversible depopulation which is characterized by the changeover time τ_{ch}. On the other hand, it reduces quantum coherent effects, and this can hinder the short-time depopulation. It is tempting to define a time τ_{coh} defining the timescale of quantum coherent effects. In our model, the lower limit of τ_{coh} is given by the vibrational period of the high-frequency mode $\tau_x = 2\pi/\omega_x = 25.7$ fs, but τ_{coh} can be higher due to the strong vibronic effects (see below). For $\tau_{ch} > \tau_{coh}$, vibrational/vibronic coherent effects contribute significantly and the changeover time is clearly visible. If, however, $\tau_{ch} < \tau_{coh}$, then depopulation always increases with temperature.

Panel b) of Fig. 1 displays $p_1(t)$ for a relatively strong vibronic coupling $\alpha = 300$ cm^{-1}. The comparison of panels a) and b) reveals that increasing α has a profound effect on the population evolution. First, Zeno times are shortened: $\tau_Z = 12.5$ for continuous lines and $\tau_Z = 5.8$ for dashed lines (see the inset). Second, stronger α diminishes the impact of static disorder (continuous/dashed lines of different color are quite similar, notably at $T = 300$ K). Third, temperature always facilitates the $p_1(t)$ depopulation (continuous lines are above dashed lines of the same color). We thus conclude that the characteristic time τ_{ch} significantly decreases with α, becoming comparable to or shorter than τ_{coh} for a broad range of temperatures.

Fig. 2 depicts populations of site number 4, $p_4(t)$, for the same set of parameters as in Fig. 1. Obviously, $p_4(0) = 0$ and it takes some time to populate this site (peculiarities of

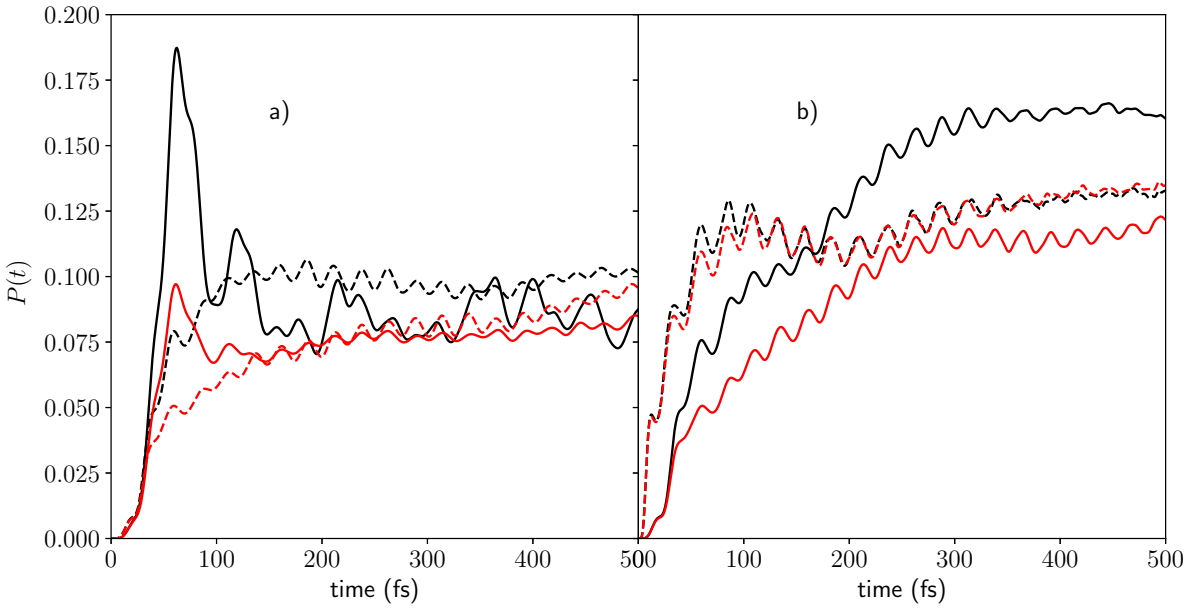

FIG. 2. Same as in Fig. 1 but for the population of site 4, $p_4(t)$.

the population transfer along the chain are considered in detail below). At longer times, populations in both panels of Fig. 2 exhibit a similar tendency: $p_4(t)$ decreases with static disorder (black lines are above red lines), which is a manifestation of the disorder-induced localization and is fully consistent with the behavior of $p_1(t)$. To elucidate temperature effects, it is worthwhile to consider the weak a) and relatively strong b) vibronic couplings separately.

$p_4(t)$ at $T = 0$ K in Fig. 2 a) exhibits high-amplitude oscillations of vibronic character with a characteristic time $\tau_{coh} \simeq 60$ fs (continuous lines). This reflects importance of quantum coherent effects in low-temperature transport. An increase in temperature substantially suppresses these coherent effects (dashed lines). The characteristic changeover times discussed above can clearly be established for $p_4(t)$ in panel a) of Fig. 2. Furthermore, the corresponding τ_{ch} for $p_1(t)$ and $p_4(t)$ are quite close (cf. panels a) in Figs. 1 and 2). If we turn to Fig. 2 b), two aspects should be pointed out. First, stronger α substantially quenches high-amplitude vibronic oscillations in $p_4(t)$. Second, the changeover time $\tau_{ch} \approx 170$ fs can clearly be established for $\sigma = 0$ (black lines in Fig. 2(b)). Under the same conditions, $p_1(t)$ in Fig. 1(b) does not exhibit any changeover effect.

It should be pointed out that $p_k(t)$ in Figs. 1 and 2 (as well as $\Pi(t)$ and $\sqrt{m_2(t)}$ in the

figures below) exhibit low-amplitude oscillations with a period around 26 fs revealing the high-frequency vibrational mode ω_x. These oscillations persist for observables calculated without (black lines) and with (red lines) averaging over static disorder. This behavior is fully consistent with the predictions of Refs.[18,19] which demonstrate that dynamical variables averaged over static disorder with a characteristic dispersion σ exhibit predominantly vibrational oscillations at times $t > 2\pi/\sigma$:

$$p_k(t) \approx \sum_{k=x,y} \sum_{m=0}^{M_k} a_{km}(t) \cos(m\omega_k t - \varphi_{km}(t)). \tag{25}$$

Here $a_{km}(t)$, $\varphi_{km}(t)$ are some slowly varying functions of time, and M_k is the maximal number of overtones for the kth vibrational mode. Despite strong electron-vibrational coupling described by the Hamiltonian of Eq. (21), vibrational coherences featuring the fundamental of the high-frequency vibrational mode ω_x survive averaging over static disorder and are clearly visible in evolutions of $p_k(t)$, $\Pi(t)$, and $m_2(t)$ considered in the present work. It should be noted that the high-frequency modes x_n are the tuning modes and the low-frequency modes y_n are the coupling modes shaping the conical intersections between the neighboring sites in the SSH model. The potential energy functions of the tuning modes in excited electronic states are normally shifted with respect to the potential energy functions in the electronic ground state (parameter g of the SSH model), while the corresponding potential energy functions of the coupling modes are not shifted. Due to that, the tuning modes are manifested in the electronic population evolutions and their probability densities exhibit a high-amplitude wave-packet motion, while the coupling modes are not manifested in population evolutions, and their wavepackets exhibit a characteristic pulsating motion[59,60].

Fig. 3 shows the IPR $\Pi(t)$ as a function of time for relatively weak ($\sigma = 100$ cm^{-1}, panel a)) and strong ($\sigma = 300$ cm^{-1}, panel b)) static disorder at $T = 0$ K (continuous lines), $T = 300$ K (dashed lines), weak ($\alpha = 100$ cm^{-1}, black lines) and relatively strong ($\alpha = 300$ cm^{-1}, red lines) vibronic coupling. For $\alpha = 300$ cm^{-1}, temperature always increases delocalization: red dashed lines are above continuous red lines, and static disorder does not have significant effect on the $\Pi(t)$ behavior. For $\alpha = 100$ cm^{-1}, the IPR dynamics is more complex.

Let us first inspect $\Pi(t)$ for weak static disorder (panel a) of Fig. 3). Apart from the low-amplitude vibrational beatings, delocalization clearly increases with time, though almost saturates for $\alpha = 300$ cm^{-1}(red lines). For $\alpha = 100$ cm^{-1}, $\Pi(t)$ tends to the limiting value

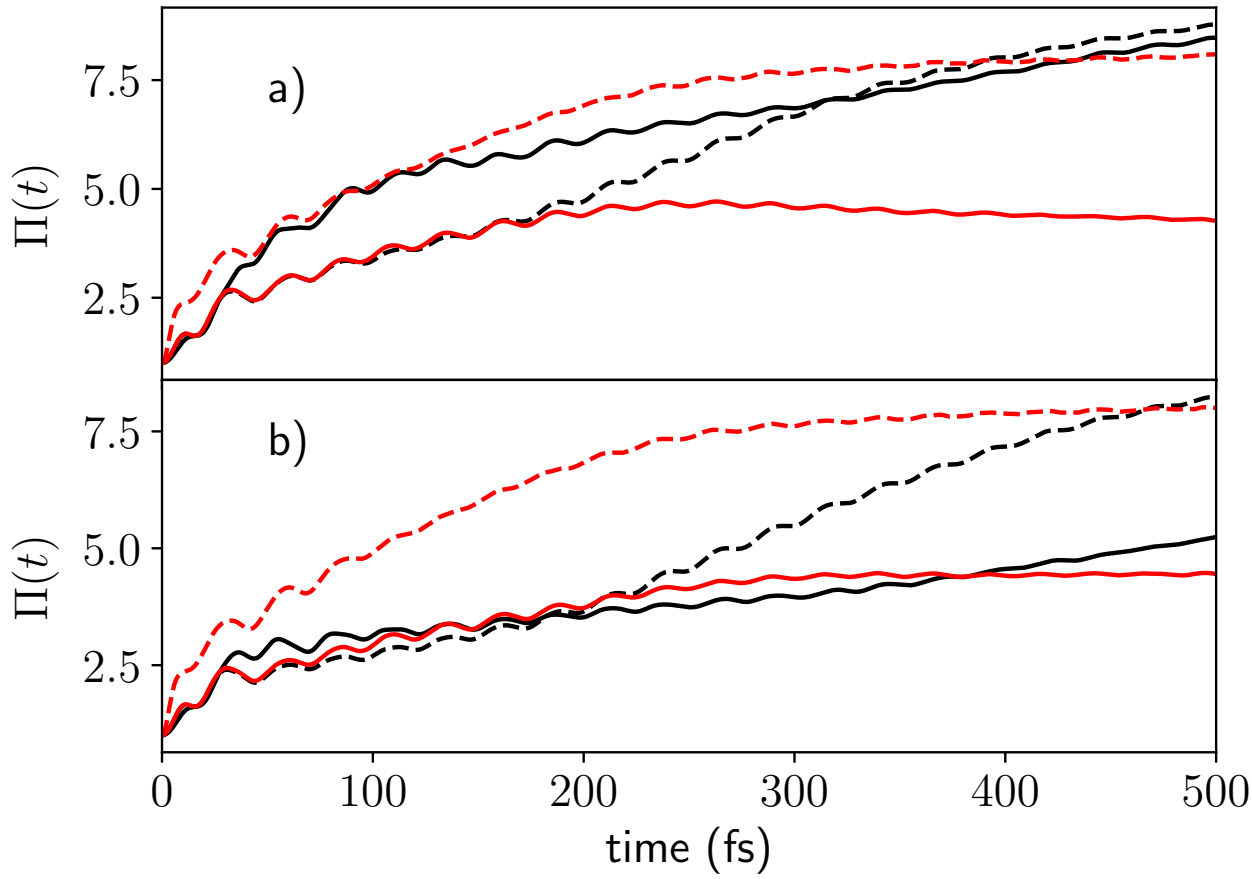

FIG. 3. IPR $\Pi(t)$ for $T = 0$, $\alpha = 100$ cm^{-1}(continuous black line), $T = 300$ K, $\alpha = 100$ cm^{-1}(dashed black line), $T = 0$, $\alpha = 300$ cm^{-1}(continuous red line), and $T = 300$ K, $\alpha = 300$ cm^{-1}(dashed red line). For panel a), $\sigma = 0$. For panel b), $\sigma = 300$ cm^{-1}.

of $N_{el} = 10$, indicating an almost complete delocalization over 10 sites (black lines). When $\alpha = 300$ cm^{-1}and $T = 0$, $\Pi(t)$ reaches a value of 5 (continuous red line) showing that dynamic disorder induced by the vibronic coupling increases the long-time localization (and therefore decreases delocalization) at low temperatures. At $T = 0$ and $\alpha = 100$ cm^{-1}, $\Pi(t)$ exhibits a changeover around $\tau_{ch} \approx 300$ fs (cf. continuous an dashed black lines). This is the manifestation of the dual effect of temperature discussed above. The value of the changeover time is close to the corresponing value $\tau_{ch} \approx 270$ for $p_1(t)$. Panel b) displays $\Pi(t)$ for $\sigma = 300$ cm^{-1}. We clearly observe that for $\alpha = 100$ cm^{-1}(black curves) the increase of static disorder significantly decreases the maximum IPR values and shortens the changeover time to 170

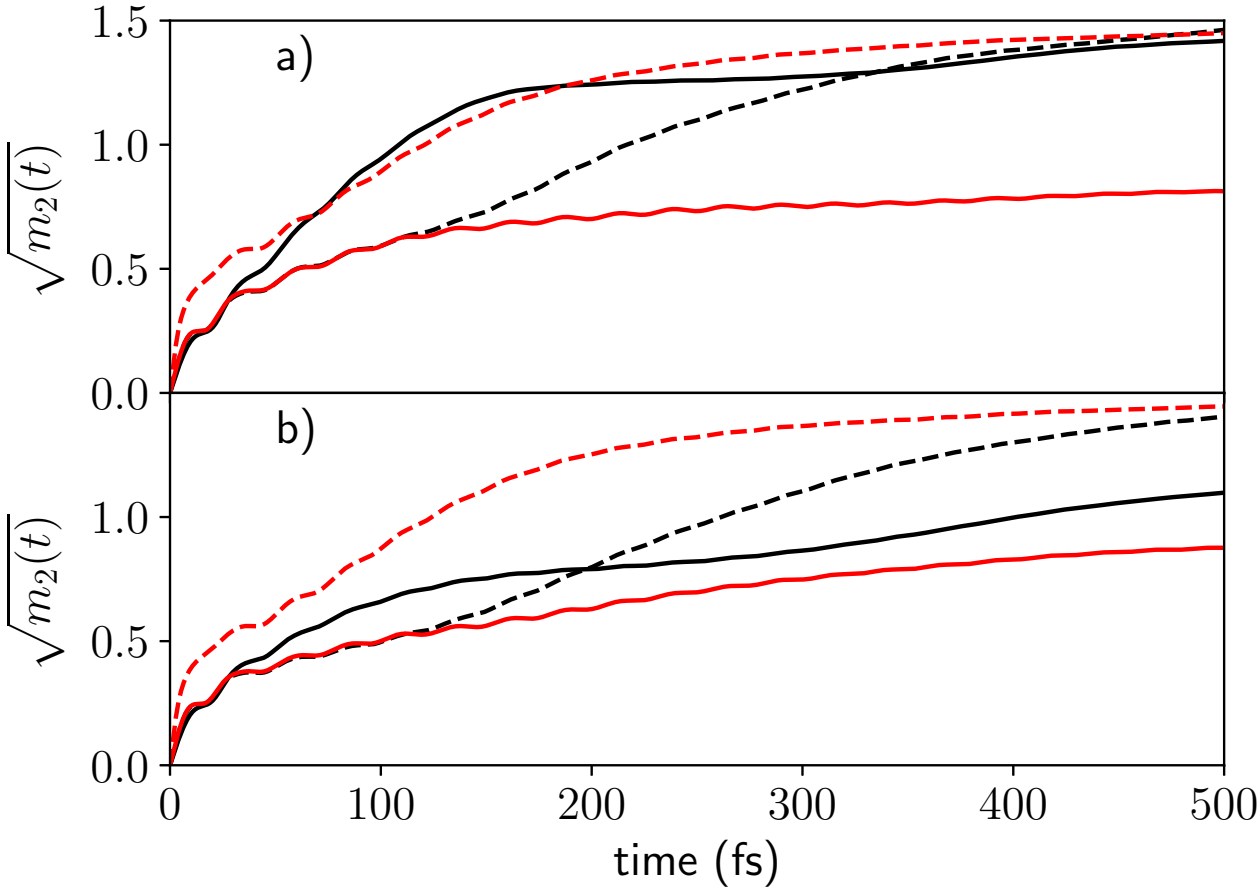

FIG. 4. $\sqrt{m_2(t)}$ for $T = 0$, $\alpha = 100$ cm^{-1}(continuous black line), $T = 300$ K, $\alpha = 100$ cm^{-1}(dashed black line), $T = 0$, $\alpha = 300$ cm^{-1}(continuous red line), and $T = 300$ K, $\alpha = 300$ cm^{-1}(dashed red line). For panel a), $\sigma = 0$. For panel b), $\sigma = 300$ cm^{-1}.

fs, which is again consistent with $\tau_{ch} \approx 150$ fs for $p_1(t)$.

Finally, the square of the second moment, $\sqrt{m_2(t)}$, is plotted in Fig. 4 for $\sigma = 100$ cm^{-1} a) and $\sigma = 300$ cm^{-1} b). Continuous (dashed) lines correspond to $T = 0$ (300 K), while black (red) lines correspond to $\alpha = 100$ cm^{-1} (300 cm^{-1}). Interestingly, $\sqrt{m_2(t)}$ does not exhibit ballistic regime for any parameter set and for any time interval. For $T = 0$, $\alpha = 100$ cm^{-1} and relatively weak disorder (continuous black line in panel a)), $\sqrt{m_2(t)}$ clearly shows two regimes: $\sqrt{m_2(t)} \sim t^{0.55}$ for $300 > t > 30$ fs and $\sqrt{m_2(t)} \sim t^{0.2}$ for $1000 > t > 300$ fs. All remaining second moments cannot be approximated by a power low with constant exponent, but definitely correspond to the anomalous diffusion regime, exhibiting scaling

$\sim t^{\nu(t)}$ with $\nu(t) < 0.2$. Static disorder does not produce significant effect on $\sqrt{m_2(t)}$ in the case of strong vibronic coupling $\alpha = 300$ cm^{-1}(cf. red lines in panels a) and b)), while temperature always increases $\sqrt{m_2(t)}$. This is fully consistent with the IPR behavior. For $\alpha = 100$ cm^{-1}, on the other hand, $\sqrt{m_2(t)}$ exhibits a changeover at around 320 fs a) and 200 fs b), which, again, are consistent with the corresponding τ_{ch} for $p_1(t)$.

V. DISCUSSION AND CONCLUSIONS

By exploiting finite-temperature representation of the Schrödinger equation, we have developed a computationally efficient and numerically accurate wavefunction-based approach for the evaluation of quantum observables averaged over static disorder, $\mathcal{A}(t)$. In this approach static-disorder variables are incorporated into the system Hamiltonian and treated as harmonic modes modifying the electronic parameters of the system. These static disorder modes are thus handled on equal footing with the system vibrational modes responsible for dynamic disorder. If N_{el}, N_v, and N_Ω denote the number of the electronic, vibrational, and static disorder DoFs in the system, then traditional evaluation of $\mathcal{A}(t)$ requires M_Ω propagations of the density matrix for the system with N_{el} electronic and N_v vibrational DoFs, where $M_\Omega \gg N_\Omega$ is the number of Monte Carlo samplings necessary for the calculation of the N_Ω-dimensional integral. The methodology developed in the present work requires just a single propagation of the wave function of the system with N_{el} electronic and $2N_v + N_\Omega$ vibrational DoFs, leading to huge computational savings. In conjunction with TT decomposition techniques for the solution of the TFD Schrödinger equation, the methodology of the present work enables the treatment of static disorder with a minimal computational cost for a large number of multidimensional problems.

In the present work, we have made the standard assumption that electronic parameters ε_{nm} of the system Hamiltonian H_Ω are linear in static disorder variables Ω_j. However, the methodology remains valid for any dependence of H_Ω on Ω_j. In addition, the dynamical variable A can also be an arbitrary function of Ω_j. The assumption about independent static disorder variables can also be relaxed, if necessary: a simple diagonalization of the quadratic form in the multidimensional Gaussian distribution introduces normal disorder modes which can be directly handled by the method of the present work.

The developed method of averaging over static disorder is not limited to the TFD repre-

sentation. Without alterations, it can be incorporated into any wavefunction/ density matrix/ stochastic description of quantum dynamics governed by the multidimensional electron-vibrational VC Hamiltoninas. For example, it looks promising to combine the present static disorder averaging technique with multi-configuration time-dependent Hartree method,[61–63] Davydov Ansatz method,[64–67] multiconfigurational Ehrenfest method,[68–70] time-dependent density matrix renormalization group method,[71–75] variants of MPS/TT,[76–78] recent modifications of real-time path integral techniques[79–81] and with the machinery for the solution of hierarchy equations of motion recently developed in Refs.[82–86] Work in this direction is currently in progress.

DATA AVAILABILITY

The data that support the findings of this study are available from the corresponding author upon reasonable request.

VI. ACKNOWLEDGMENTS

M.F.G. acknowledges support of Hangzhou Dianzi University through startup funding. R. B. acknowledges support from the European Union's Horizon 2020 research and innovation programme under grant agreement No. 826013 as well as support from the University of Torino through the local research funding Grant No. BORR-RILO-18-01 and BORR-RILO-19-01.

Appendix A: TFD formalism in the presence of static disorder

Let us introduce the eigenvectors of the vibrational Hamiltonian,

$$\sum_l \omega_l a_l^\dagger a_l |\boldsymbol{k}\rangle = E_{\boldsymbol{k}} |\boldsymbol{k}\rangle.$$

Obviously,

$$|\boldsymbol{k}\rangle = \prod_l |k_l\rangle, \quad E_{\boldsymbol{k}} = \sum_l k_l \omega_l \tag{A1}$$

where $|k_l\rangle$ are the eigenvectors of the lth harmonic mode. We also define vectors $|\tilde{\boldsymbol{k}}\rangle$ which are a copy of the original vectors $|\boldsymbol{k}\rangle$ but belong to the so-called *tilde* Hilbert space. Adopting

the notation

$$|\boldsymbol{k}\tilde{\boldsymbol{k}}\rangle = |\boldsymbol{k}\rangle|\tilde{\boldsymbol{k}}\rangle,$$

we introduce the unit vector in the $|\boldsymbol{k}\rangle \otimes |\tilde{\boldsymbol{k}}\rangle$ vector space,

$$|\boldsymbol{I}_v\rangle = \sum_{\boldsymbol{k}} |\boldsymbol{k}\tilde{\boldsymbol{k}}\rangle, \tag{A2}$$

and the so-called thermal vacuum state,

$$|\mathbf{0}_v(\beta)\rangle = \sqrt{\rho_v}|\boldsymbol{I}_v\rangle = Z_v^{-\frac{1}{2}} e^{-\frac{1}{2}\sum_l \omega_l a_l^\dagger a_l}|\boldsymbol{I}_v\rangle. \tag{A3}$$

With the above definitions, the thermal Boltzmann distribution of Eq. (5) can be rewritten in the form

$$\rho_v = \mathrm{Tr}_{\tilde{\boldsymbol{k}}}\{|\mathbf{0}_v(\beta)\rangle\langle\mathbf{0}_v(\beta)|\} \tag{A4}$$

where $\mathrm{Tr}_{\tilde{\boldsymbol{k}}}\{...\}$ denotes the trace over the tilde subspace. The equivalence of Eqs. (5) and (A4) follows immediately from the orthogonality of the harmonic oscillator eigenvectors.

Let us now consider the Liouville – von Neumann equation

$$\partial_t \sigma_\Omega(t) = -i[H_\Omega, \sigma_\Omega(t)] \tag{A5}$$

driven by the Hamiltonian H_Ω of Eq. (7) and evaluated with the initial condition

$$\sigma_\Omega(0) = |e\rangle\langle e| \otimes |0_\Omega\rangle\langle 0_\Omega| \otimes |\mathbf{0}_v(\beta)\rangle\langle\mathbf{0}_v(\beta)|. \tag{A6}$$

Eq. (A4) guarantees that the system density matrix $\rho_\Omega(t)$ satisfying the original Liouville – von Neumann equation (3) with the initial condition of Eq. (4) is given by

$$\rho_\Omega(t) = \mathrm{Tr}_{\tilde{\boldsymbol{k}}}\{\sigma_\Omega(t)\}. \tag{A7}$$

Furthermore, it is easy to verify that any Liouville – von Neumann equation of the form

$$\partial_t \sigma_\Omega(t) = -i[H_\Omega - \tilde{h}_v, \sigma_\Omega(t)] \tag{A8}$$

$\tilde{h}_v$ being any operator acting in the tilde subspace only, together with the initial condition (4) fulfills Eq. (A7).

Since the initial condition of Eq. (A6) corresponds to a pure state in the extended Hilbert space, the solution of Eq. (A8) reads

$$\sigma_\Omega(t) = |\psi_\Omega(t)\rangle\langle\psi_\Omega(t)| \tag{A9}$$

where the wave function $|\psi_\Omega(t)\rangle$ obeys the TFD Schrödinger equation

$$\partial_t|\psi_\Omega(t)\rangle = -i\hat{H}_\Omega|\psi_\Omega(t)\rangle \tag{A10}$$

with the extended Hamiltonian

$$\hat{H}_\Omega = H_\Omega - \tilde{h}_v \tag{A11}$$

and the initial condition

$$|\psi_\Omega(0)\rangle = |e\rangle|0_\Omega\rangle|\mathbf{0}_v(\beta)\rangle. \tag{A12}$$

We have thus demonstrated that the solution of the original Liouville – von Neumann equation (3) with the initial condition (4) is equivalent to the solution of the TFD Schrödinger equation (A10) with the initial condition (A12).

The key advantage of the TFD machinery is a compact analytical representation of the thermal vacuum state given by thermal Bogoliubov transformation

$$e^{-iG}|\mathbf{0}_v\tilde{\mathbf{0}}_v\rangle = |\mathbf{0}_v(\beta)\rangle \tag{A13}$$

where $|\mathbf{0}_v\tilde{\mathbf{0}}_v\rangle$ is the ground state in the $|\boldsymbol{k}\rangle \otimes |\tilde{\boldsymbol{k}}\rangle$ subspace. Applying the inverse thermal Bogoliubov transformation to Eq. (A10), we obtain the TFD Schrödinger equation (15) in which

$$H_\theta = e^{iG}\hat{H}_\Omega e^{-iG} \tag{A14}$$

and

$$\big|\psi_\theta(t)\big\rangle = e^{iG}\big|\psi_\Omega(t)\big\rangle. \tag{A15}$$

Hence the expectation value of any quantum observable A averaged over static disorder is given by Eq. (14) where

$$A_\theta = e^{iG}Ae^{-iG}. \tag{A16}$$

For thermal vacuum state $|\mathbf{0}_v(\beta)\rangle$ of Eq. (A3), the operator of thermal Bogoliubov transformation reads[13,87–90]

$$G = -i\sum_j \theta_j(a_j\tilde{a}_j - a_j^\dagger\tilde{a}_j^\dagger) \tag{A17}$$

where θ_j are defined per Eq. (13). The explicit form of the transformed Hamiltonian H_θ, can then be easily obtained by making a common assumption that the electronic terms ε_{nm}

are independent of nuclear DoFs coordinates.[25–28] By choosing

$$\tilde{h}_v = \sum_k \omega_k \tilde{a}_k^\dagger \tilde{a}_k$$

and using the fundamental relations[13]

$$e^{iG} a_j e^{-iG} = a_j \cosh(\theta_j) + \tilde{a}_j^\dagger \sinh(\theta_j), \tag{A18}$$

$$e^{iG} \tilde{a}_j e^{-iG} = \tilde{a}_j \cosh(\theta_j) + a_j^\dagger \sinh(\theta_j). \tag{A19}$$

we obtain the Hamiltonian of Eq. (12).

REFERENCES

[1]R. Kubo, M. Toda, and N. Hashitsume, en*Statistical Physics II: Nonequilibrium Statistical Mechanics*, 2nd ed., Springer Series in Solid-State Sciences, Springer Ser.Solid-State Statistical Physics (Springer-Verlag, Berlin Heidelberg, 1991).

[2]J.-L. Brédas, E. H. Sargent, and G. D. Scholes, en"Photovoltaic concepts inspired by coherence effects in photosynthetic systems," Nat Mater **16**, 35–44 (2017).

[3]J. M. Moix, M. Khasin, and J. Cao, en"Coherent quantum transport in disordered systems: I. The influence of dephasing on the transport properties and absorption spectra on one-dimensional systems," New J. Phys. **15**, 085010 (2013).

[4]P. Kramer, en"A review of the time-dependent variational principle," J. Phys.: Conf. Ser. **99**, 012009 (2008).

[5]Y. Tanimura, "Numerically "exact" approach to open quantum dynamics: The hierarchical equations of motion (HEOM)," J. Chem. Phys. **153**, 020901 (2020).

[6]Y. Tanimura, "Stochastic Liouville, Langevin, Fokker–Planck, and Master Equation Approaches to Quantum Dissipative Systems," J. Phys. Soc. Jpn. **75**, 082001 (2006).

[7]M. Thoss and H. Wang, "Quantum dynamical simulation of ultrafast molecular processes in the condensed phase," Chem. Phys. **322**, 210–222 (2006).

[8]C. Chuang and J. Cao, "Universal Scalings in Two-Dimensional Anisotropic Dipolar Excitonic Systems," Phys. Rev. Lett. **127**, 047402 (2021).

[9]R. Borrelli and M. F. Gelin, "Quantum electron-vibrational dynamics at finite temperature: Thermo field dynamics approach," J. Chem. Phys. **145**, 224101 (2016).

[10]R. Borrelli and M. F. Gelin, En"Simulation of Quantum Dynamics of Excitonic Systems at Finite Temperature: An efficient method based on Thermo Field Dynamics," Sci. Rep. **7**, 9127 (2017).

[11]R. Borrelli, "Theoretical study of charge-transfer processes at finite temperature using a novel thermal Schrödinger equation," Chemical Physics Ultrafast Photoinduced Processes in Polyatomic Molecules:Electronic Structure, Dynamics and Spectroscopy (Dedicated to Wolfgang Domcke on the Occasion of His 70th Birthday), **515**, 236–241 (2018).

[12]L. Chen and Y. Zhao, "Finite temperature dynamics of a Holstein polaron: The thermo-field dynamics approach," J. Chem. Phys. **147**, 214102 (2017).

[13]Y. Takahashi and H. Umezawa, "Thermo field dynamics," Int. J. Mod. Phys. B **10**, 1755–1805 (1996).

[14]T. Arimitsu, "General Formulation for Open Systems –Mirror Operation–," J. Phys. Soc. Jpn. **51**, 1720–1726 (1982).

[15]I. Oseledets and E. Tyrtyshnikov, "Breaking the Curse of Dimensionality, Or How to Use SVD in Many Dimensions," SIAM J. Sci. Comput. **31**, 3744–3759 (2009).

[16]R. Borrelli and M. F. Gelin, en"Finite temperature quantum dynamics of complex systems: Integrating thermo-field theories and tensor-train methods," WIREs Comput. Mol. Sci. **n/a**, e1539 (2021).

[17]Gelin Maxim F. and Borrelli Raffaele, "Thermal Schrödinger Equation: Efficient Tool for Simulation of Many-Body Quantum Dynamics at Finite Temperature," Annalen der Physik **529**, 1700200 (2017).

[18]M. F. Gelin and R. Borrelli, "Simulation of Nonlinear Femtosecond Signals at Finite Temperature via a Thermo Field Dynamics-Tensor Train Method: General Theory and Application to Time- and Frequency-Resolved Fluorescence of the Fenna–Matthews–Olson Complex," J. Chem. Theory Comput. (2021).

[19]M. F. Gelin, R. Borrelli, and W. Domcke, "Origin of Unexpectedly Simple Oscillatory Responses in the Excited-State Dynamics of Disordered Molecular Aggregates," J. Phys. Chem. Lett. **10**, 2806–2810 (2019).

[20]R. Kubo, "Stochastic Liouville Equations," J. Math. Phys. **4**, 174–183 (1963).

[21]R. Orús, "A practical introduction to tensor networks: Matrix product states and projected entangled pair states," Annals of Physics **349**, 117–158 (2014).

[22]I. Oseledets, "Tensor-Train Decomposition," SIAM J. Sci. Comput. **33**, 2295–2317 (2011).

[23]C. Lubich, I. Oseledets, and B. Vandereycken, "Time Integration of Tensor Trains," SIAM J. Numer. Anal. **53**, 917–941 (2015).

[24]S. Paeckel, T. Köhler, A. Swoboda, S. R. Manmana, U. Schollwöck, and C. Hubig, en"Time-evolution methods for matrix-product states," Annals of Physics **411**, 167998 (2019).

[25]W. Domcke and G. Stock, en"Theory of Ultrafast Nonadiabatic Excited-State Processes and their Spectroscopic Detection in Real Time," in en*Advances in Chemical Physics*, Vol. 100 (John Wiley & Sons, Ltd, 1997) pp. 1–169.

[26]H. Köppel, W. Domcke, and L. S. Cederbaum, "Multimode Molecular Dynamics Beyond the Born-Oppenheimer Approximation," in *Advances in Chemical Physics*, Vol. 57 (John Wiley & Sons, Inc., Hoboken, NJ, USA, 1984) pp. 59–246.

[27]S. Mukamel and D. Abramavicius, "Many-Body Approaches for Simulating Coherent Nonlinear Spectroscopies of Electronic and Vibrational Excitons," Chem. Rev. **104**, 2073–2098 (2004).

[28]D. Abramavicius, B. Palmieri, D. V. Voronine, F. Šanda, and S. Mukamel, "Coherent Multidimensional Optical Spectroscopy of Excitons in Molecular Aggregates; Quasiparticle versus Supermolecule Perspectives," Chem. Rev. **109**, 2350–2408 (2009).

[29]R. Borrelli and W. Domcke, "First-principles study of photoinduced electron-transfer dynamics in a Mg–porphyrin–quinone complex," Chem. Phys. Lett. **498**, 230–234 (2010).

[30]R. Borrelli, M. Di Donato, and A. Peluso, "Electron transfer rates and Franck–Condon factors: An application to the early electron transfer steps in photosynthetic reaction centers," Theor. Chem. Acc. Theory Comput. Model. Theor. Chim. Acta **117**, 957–967 (2007).

[31]N. J. Hestand and F. C. Spano, "Expanded theory of H- and J- molecular aggregates: The effects of vibronic coupling and intermolecular charge transfer," Chem. Rev. **118**, 7069–7163 (2018).

[32]D. Chen, J. Ye, H. Zhang, and Y. Zhao, "On the Munn-Silbey approach to polaron transport with off-diagonal coupling and temperature-dependent canonical transformations," J. Phys. Chem. B **115**, 5312–5321 (2011).

[33]H. Oberhofer, K. Reuter, and J. Blumberger, "Charge transport in molecular materials: An assessment of computational methods," Chem. Rev. **117**, 10319–10357 (2017).

[34]F. Plasser, S. Gómez, M. F. S. J. Menger, S. Mai, and L. González, en"Highly efficient

surface hopping dynamics using a linear vibronic coupling model," Phys. Chem. Chem. Phys. **21**, 57–69 (2018).

[35]H. Wang, "Multilayer Multiconfiguration Time-Dependent Hartree Theory," J. Phys. Chem. A **119**, 7951–7965 (2015).

[36]S. Holtz, T. Rohwedder, and R. Schneider, en"On manifolds of tensors of fixed TT-rank," Numer. Math. **120**, 701–731 (2011).

[37]L. S. Cederbaum, E. Gindensperger, and I. Burghardt, "Short-Time Dynamics Through Conical Intersections in Macrosystems," Phys. Rev. Lett. **94**, 113003 (2005).

[38]E. Gindensperger, I. Burghardt, and L. S. Cederbaum, "Short-time dynamics through conical intersections in macrosystems. II. Applications," J. Chem. Phys. **124**, 144104 (2006).

[39]A. W. Chin, Á. Rivas, S. F. Huelga, and M. B. Plenio, "Exact mapping between system-reservoir quantum models and semi-infinite discrete chains using orthogonal polynomials," Journal of Mathematical Physics **51**, 092109 (2010).

[40]M. M. Rams and M. Zwolak, "Breaking the Entanglement Barrier: Tensor Network Simulation of Quantum Transport," Phys. Rev. Lett. **124**, 137701 (2020).

[41]S. V. Dolgov, en"A Tensor Decomposition Algorithm for Large ODEs with Conservation Laws," Comput. Methods Appl. Math. **19**, 23–38 (2019).

[42]S. M. Greene and V. S. Batista, "Tensor-Train Split-Operator Fourier Transform (TT-SOFT) Method: Multidimensional Nonadiabatic Quantum Dynamics," J. Chem. Theory Comput. **13**, 4034–4042 (2017).

[43]J. Haegeman, J. I. Cirac, T. J. Osborne, I. Pižorn, H. Verschelde, and F. Verstraete, "Time-Dependent Variational Principle for Quantum Lattices," Phys. Rev. Lett. **107**, 070601 (2011).

[44]J. Haegeman, C. Lubich, I. Oseledets, B. Vandereycken, and F. Verstraete, "Unifying time evolution and optimization with matrix product states," Phys. Rev. B **94**, 165116 (2016).

[45]J. Haegeman, T. J. Osborne, and F. Verstraete, "Post-matrix product state methods: To tangent space and beyond," Phys. Rev. B **88**, 075133 (2013).

[46]S. Ciuchi and S. Fratini, "Band Dispersion and Electronic Lifetimes in Crystalline Organic Semiconductors," Phys. Rev. Lett. **106**, 166403 (2011).

[47]A. Landi, R. Borrelli, A. Capobianco, and A. Peluso, "Transient and Enduring Electronic Resonances Drive Coherent Long Distance Charge Transport in Molecular Wires," J. Phys. Chem. Lett. **10**, 1845–1851 (2019).

[48]W. P. Su, J. R. Schrieffer, and A. J. Heeger, "Solitons in Polyacetylene," Phys. Rev. Lett. **42**, 1698–1701 (1979).

[49]A. Landi, R. Borrelli, A. Capobianco, A. Velardo, and A. Peluso, "Hole Hopping Rates in Organic Semiconductors: A Second-Order Cumulant Approach," J. Chem. Theory Comput. **14**, 1594–1601 (2018).

[50]A. Troisi and G. Orlandi, "Charge-Transport Regime of Crystalline Organic Semiconductors: Diffusion Limited by Thermal Off-Diagonal Electronic Disorder," Phys. Rev. Lett. **96**, 086601 (2006).

[51]A. Landi, A. Peluso, and A. Troisi, en"Quantitative Prediction of the Electro-Mechanical Response in Organic Crystals," Adv. Mater. **33**, 2008049 (2021).

[52]S. Fratini and S. Ciuchi, "Bandlike Motion and Mobility Saturation in Organic Molecular Semiconductors," Phys. Rev. Lett. **103**, 266601 (2009).

[53]T. Meier, Y. Zhao, V. Chernyak, and S. Mukamel, "Polarons, localization, and excitonic coherence in superradiance of biological antenna complexes," J. Chem. Phys. **107**, 3876–3893 (1997).

[54]V. Chorošajev, O. Rancova, and D. Abramavicius, en"Polaronic effects at finite temperatures in the B850 ring of the LH2 complex," Phys. Chem. Chem. Phys. **18**, 7966–7977 (2016).

[55]A. Somoza, K. Sun, R. Molina, and Y. Zhao, "Dynamics of coherence, localization and excitation transfer in disordered nanorings," Phys. Chem. Chem. Phys. **19**, 25996–26013 (2017).

[56]R. Borrelli and M. F. Gelin, en"Quantum dynamics of vibrational energy flow in oscillator chains driven by anharmonic interactions," New J. Phys. **22**, 123002 (2020).

[57]P. Facchi and S. Pascazio, en"Quantum Zeno Phenomena: Pulsed versus Continuous Measurement," Fortschritte Phys. **49**, 941 (2001).

[58]K. Sun, Q. Xu, L. Chen, M. F. Gelin, and Y. Zhao, "Temperature effects on singlet fission dynamics mediated by a conical intersection," J. Chem. Phys. **153**, 194106 (2020).

[59]L. Chen, M. F. Gelin, and W. Domcke, "Multimode quantum dynamics with multiple Davydov D_2 trial states: Application to a 24-dimensional conical intersection model," J. Chem. Phys. **150**, 024101 (2019).

[60]K. Sun, W. Xie, L. Chen, W. Domcke, and M. F. Gelin, "Multi-faceted spectroscopic mapping of ultrafast nonadiabatic dynamics near conical intersections: A computational

study," J. Chem. Phys. **153**, 174111 (2020).

[61]H. Wang and M. Thoss, "Nonperturbative quantum simulation of time-resolved nonlinear spectra: Methodology and application to electron transfer reactions in the condensed phase," Chem. Phys. **347**, 139–151 (2008).

[62]W. Popp, D. Brey, R. Binder, and I. Burghardt, "Quantum dynamics of exciton transport and dissociation in multichromophoric systems," Annu. Rev. Phys. Chem. **72**, 591–616 (2021).

[63]F. Di Maiolo, G. A. Worth, and B. Irene, "Multi-layer Gaussian-based multi-configuration time-dependent Hartree (ML-GMCTDH) simulations of ultrafast charge separation in a donor–acceptor complex," J. Chem. Phys. **154**, 144106 (2021).

[64]K. W. Sun, M. F. Gelin, V. Y. Chernyak, and Y. Zhao, "Davydov Ansatz as an efficient tool for the simulation of nonlinear optical response of molecular aggregates," J. Chem. Phys. **142**, 212448 (2015).

[65]L. Wang, Y. Fujihashi, L. Chen, and Y. Zhao, "Finite-temperature time-dependent variation with multiple Davydov states," J. Chem. Phys. **146**, 124127 (2017).

[66]M. Werther, F. Grossmann, Z. Huang, and Y. Zhao, "Davydov-Ansatz for Landau-Zener-Stueckelberg-Majorana transitions in an environment: Tuning the survival probability via number state excitation," J. Chem. Phys. **150**, 234109 (2021).

[67]K. Sun, X. Liu, W. Hu, M. Zhang, G. Long, and Y. Zhao, "Singlet fission dynamics and optical spectra of pentacene and its derivatives," Phys. Chem. Chem. Phys. **23**, 12654–12667 (2021).

[68]L. Chen, M. F. Gelin, and D. V. Shalashilin, "Dynamics of a one-dimensional holstein polaron: The multiconfigurational Ehrenfest method," J. Chem. Phys. **151**, 244116 (2019).

[69]L. Chen, K. Sun, D. Shalashilin, M. F. Gelin, and Y. Zhao, "Efficient simulation of time- and frequency-resolved four-wave-mixing signals with multiconfigurational Ehrenfest approach," J. Chem. Phys. **153**, 174111 (2021).

[70]L. Chen, R. Borrelli, D. V. Shalashilin, Y. Zhao, and M. F. Gelin, "Simulation of time- and frequency-resolved four-wave-mixing signals at finite temperatures: A thermo-field dynamics approach," J. Chem. Theory Comput. **17**, 4359–4373 (2021).

[71]J. Ren, Z. Shuai, and G. K.-L. Chan, "Time-dependent density matrix renormalization group algorithms for nearly exact absorption and fluorescence spectra of molecular aggregates at both zero and finite temperature," J. Chem. Theory Comput. **14**, 5027–5039

(2018).

[72]T. Jiang, W. Li, J. Ren, and Z. Shuai, "Finite temperature dynamical density matrix renormalization group for spectroscopy in frequency domain," J. Phys. Chem. Lett. **11**, 3761–3768 (2020).

[73]A. Baiardi and M. Reiher, "Large-scale quantum dynamics with matrix product states," J. Chem. Theory Comput. **15**, 3481–3498 (2019).

[74]X. Xie, Y. Liu, Y. Yao, U. Schollwöck, C. Liu, and H. Ma, "Time-dependent density matrix renormalization group quantum dynamics for realistic chemical systems," J. Chem. Phys. **151**, 224101 (2019).

[75]D. Jansen, J. Bonc, and F. Heidrich-Meisner, "Finite-temperature density-matrix renormalization group method for electron-phonon systems: Thermodynamics and holstein-polaron spectral functions," Phys. Rev. B **102**, 165155 (2020).

[76]S. M. Greene and V. S. Batista, "Tensor-train split-operator fourier transform (TT-SOFT) method: Multidimensional nonadiabatic quantum dynamics," J. Chem. Theory Comput. **13**, 4034–4042 (2017).

[77]F. A. Schröder, D. H. Turban, N. D. Musser, Andrew J. Hine, and A. W. Chin, "Tensor network simulation of multi-environmental open quantum dynamics via machine learning and entanglement renormalisation," Nat. Comm. **10**, 1062 (2019).

[78]A. Nü ßeler, I. Dhand, and M. B. Huelga, S. F. Plenio, "Efficient construction of matrix-product representations of many-body gaussian states," Phys. Rev. A **104**, 012415 (2021).

[79]S. Kundu and N. Makri, "Real-time path integral simulation of exciton-vibration dynamics in light-harvesting bacteriochlorophyll aggregates," J. Phys. Chem. Lett. **11**, 8783–8789 (2020).

[80]S. Kundu and N. Makri, "Modular path integral for fi nite-temperature dynamics of extended systems with intramolecular vibrations," J. Chem. Phys. **118**, 044124 (2020).

[81]S. Kundu and N. Makri, "Exciton–vibration dynamics in J-aggregates of a perylene bisimide from real-time path integral calculations," J. Phys. Chem. C **125**, 201–210 (2021).

[82]R. Borrelli, "Density matrix dynamics in twin-formulation: An efficient methodology based on tensor-train representation of reduced equations of motion," J. Chem. Phys. **150**, 234102 (2019).

[83]R. Borrelli and S. Dolgov, "Expanding the Range of Hierarchical Equations of Motion by Tensor-Train Implementation," J. Phys. Chem. B (2021).

[84]Q. Shi, Y. Xu, Y. Yan, and M. Xu, "Efficient propagation of the hierarchical equations of motion using the matrix product state method," The Journal of Chemical Physics **148**, 174102 (2018).

[85]Y. Yan, T. Xing, and Q. Shi, "A new method to improve the numerical stability of the hierarchical equations of motion for discrete harmonic oscillator modes," J. Chem. Phys. **153**, 204109 (2020).

[86]Y. Yan, M. Xu, T. Li, and Q. Shi, en"Efficient propagation of the hierarchical equations of motion using the Tucker and hierarchical Tucker tensors," J. Chem. Phys. **154**, 194104 (2021).

[87]H. Umezawa, H. Matsumoto, and M. Tachiki, *Thermo Field Dynamics and Condensed States* (North-Holland, Netherlands, 1982).

[88]I. Ojima, "Gauge fields at finite temperatures—"Thermo field dynamics" and the KMS condition and their extension to gauge theories," Annals of Physics **137**, 1–32 (1981).

[89]M. Suzuki, "Density matrix formalism, double-space and thermo field dynamics in non-equilibrium dissipative systems," Int. J. Mod. Phys. B **05**, 1821–1842 (1991).

[90]D. S. Kosov, "Nonequilibrium Fock space for the electron transport problem," J. Chem. Phys. **131**, 171102 (2009).